Article
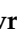
Highly Porous Cyanometallic Spin-Crossover Frameworks Employing Pyridazino[4,5-d]pyridazine Bridge

Volodymyr M. Hiiuk [1] [ID], **Sergiu Shova** [2,3] [ID], **Kostiantyn V. Domasevitch** [1] and **Il'ya A. Gural'skiy** [1,*]

1   Department of Chemistry, Taras Shevchenko National University of Kyiv, 64 Volodymyrska St., 01601 Kyiv, Ukraine
2   CEEC Institute, Ningbo University of Technology, No. 201, Fenghua Road, Ningbo 315211, China
3   "Petru Poni" Institute of Macromolecular Chemistry, 41A Aleea Gr. Ghica Voda, 700487 Iasi, Romania
*   Correspondence: illia.guralskyi@univ.kiev.ua; Tel.: +380-44-239-33-71

Abstract: Single crystals of two spin-crossover (SCO) cyanometallic coordination polymers based on the pyridazino[4,5-d]pyridazine ligand (*pp*) of the composition $[Fe(pp)M(CN)_4]\cdot G$ (where M = Pd, Pt; G = guest molecules) were obtained by a slow diffusion technique. A single-crystal X-ray analysis showed that both compounds adopted the structure of porous 3D frameworks, consisting of heterometallic cyano-bridged layers and interlayer pillar *pp* ligands, with a total solvent accessible volume of ca. 160 $Å^3$ per iron(II) ion (about 37% of the unit cell volume). These frameworks displayed hysteretic SCO behaviour with $T_{1/2}$ of 150/190 K (heating/cooling) for Pd complex and 135/170 K (heating/cooling) for Pt complex, which was confirmed by variable-temperature SCXRD experiments. This research shows the perspective of using *pp* ligand for building porous MOFs with spin transitions.

Keywords: iron(II) complexes; spin crossover; porous coordination polymers; metal-organic frameworks; single-crystal X-ray diffraction

1. Introduction

Iron(II) spin-crossover (SCO) porous coordination polymers (PCPs) occupy a special place among the various types of metal-organic frameworks (MOFs). Iron(II) ions in such types of polymers are able to undergo a reversible switch between two different electronic states (high-spin (HS) and low-spin (LS) states) under external stimuli. This causes significant changes in various physical properties of the compound including magnetic, electrical, and mechanical properties [1–4]. SCO behaviour of PCPs is often highly sensitive to the presence of guest molecules in the framework cavities. There are already many examples of how the inclusion of both small molecules and large aromatic systems in 3D Hofmann-type PCPs shows an exceptional effect on the main SCO parameters (temperature, sharpness, completeness, hysteresis) [5,6]. Moreover, the strategy of controlled incorporation and exchange of guest molecules is effective to produce multi-step SCO materials [7–9]. Thus, the combination of SCO properties, high porosity, and structural diversity make SCO-PCPs attractive components for the design of new switchable materials. The distinct influence of guest molecules on SCO properties of PCPs may be of interest for potential chemical sensing applications [10,11].

Among the first reported SCO-PCPs, there are 2D frameworks with general formula $[Fe(L)_2(NCS)_2]\cdot$Guest, where L = some bis-monodentate pyridine-like ligand such as *trans*-1,2-di(4-pyridyl)ethylene (*dpe*) [12–15], trans-4,4′-azopyridine (*azpy*) [16,17], 2,3-bis(4′-pyridyl)-2,3-butanediol (*bpbd*) [18,19], or 1,2-bis(4′-pyridyl)-1,2-ethanediol (*bped*) [20]. Complexes of this type usually exhibit guest-dependent gradual SCO behaviour with low transition temperatures (below 200 K). The adsorption of guest molecules leads to significant changes in the coordination geometry around iron(II) centres, while the desorption causes stabilization of the HS state of the framework [13,17,20].

The most known and well-studied members of SCO-PCPs that exhibit chemo-responsive behaviour are Hofmann-type iron(II) complexes of the composition [Fe(*pz*)M(CN)$_4$] (where M = Ni, Pt, Pd; *pz* = pyrazine) [21–30]. These PCPs are 3D porous frameworks, consisting of cyano-bridged layers and interlayer pillar *pz* ligands, with hysteretic SCO around room temperature. Having high porosity, *pz* complexes are able to adsorb various guest molecules including gases [22,27,30], different organic molecules [28,29], and even chemically reactive dihalogen molecules [23,25]. Such adsorption results in different SCO behaviour depending on the guest molecules and different types of host-guest interactions. A remarkable example is the CS$_2$ molecule that stabilizes the LS state of the iron(II) sites in [Fe(*pz*)Pt(CN)$_4$], whereas the benzene molecule stabilizes the HS state. The adsorption of small molecules such as CO$_2$ and N$_2$ has practically no effect on SCO [24]. Thus, guest-induced reversible modifications can be used as an intrinsic stimulus for the fine-tuning SCO properties of a material. Other examples of bridging ligands used to design 3D Hofmann-type clathrates with [M(CN)$_4$]$^{2-}$ units are 1,4-bis(4-pyridylbutadiyne) (*bpb*) [31–33], (1*H*-1,2,4-triazole-3,5-diyl)dipyridine (*Hbpt*) [34], 4,4'-di(pyridylthio)methane (*dpsme*) [35], 1,4-bis(4-pyridylethynyl)benzene (*bpeben*) [36], bis(4-pyridyl)acetylene (*bpac*) [37–39], *azpy* [40], and *dpe* [41].

SCO-PCPs based on them also demonstrate guest-dependent SCO properties and this makes them perspective for further practical applications. For example, the [Fe(*bpb*)Pt(CN)$_4$] framework is capable hosting up to two guest aromatic molecules (such as naphthalene or nitrobenzene) per iron(II) centre [31]. The use of the [Fe(*bpac*)Pt(CN)$_4$] complex makes it possible to detect volatile organic compounds (such as mono- and polyhalogen-substituted benzenes) via changes in the spin state [39].

The use of linear [M(CN)$_2$]$^-$ (where M = Ag, Au) linkers with various pillar azine ligands is also a well-working synthetic strategy for the design of SCO-PCPs [42–51]. In contrast to complexes with square-planar [M(CN)$_4$]$^{2-}$ (where M = Ni, Pt, Pd) linkers, a 2D [Fe{M(CN)$_2$}$_2$]$_\infty$ net with larger meshes is generated here, which assumes the presence of larger solvent-accessible voids. Moreover, the use of bent pillar azine ligands, as well as the introduction of different guest molecules, tends to cause distortions in the Hofmann layer leading to symmetry breaking. This is also one of the factors of stimulating multi-step SCO in complexes [8,52–59].

Thus, π-deficient heterocyclic *N*-donor ligands are mainly used to design SCO coordination polymers. Therefore, our interest was attracted by a structurally simple, geometrically regular condensed pyridazine ligand: pyridazino[4,5-d]pyridazine (*pp*; Scheme 1), which is one of the most electron deficient systems (and can even undergo inverse electron-demand [4 + 2]-cycloadditions as a bis-azadiene) [60].
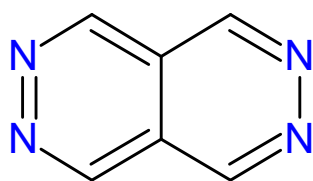
Scheme 1. Molecular structure of the pyridazino[4,5-d]pyridazine (*pp*) ligand.

Herein, we present the results in the area of SCO-PCPs. Single crystals of SCO iron(II) complexes with pillar bicyclic pyridazino[4,5-d]pyridazine ligand of the composition [Fe(*pp*)M(CN)$_4$]·G (where M = Pd (**1**), Pt (**2**); G = guest molecules) have been obtained. Both compounds adopt the structure of 3D frameworks containing guest available pores and exhibiting hysteretic SCO behaviour. Since the *pp* ligand is characterized by large distances between donor centres compared to its structural analogue, pyrazine, one could expect the formation of larger framework cavities and, consequently, an increased porosity of the obtained SCO-PCPs compared to *pz* complexes.

2. Results and Discussion

An analysis of the correlations between the SCO properties of a complex and its structure is essential for more advanced design of switchable materials; therefore, we carried out a single crystal X-ray diffraction analysis of **1** and **2** in both the LS and HS states. The corresponding crystallographic data are summarized in Table 1. The selected structural parameters are given in Table 2.

Table 1. Crystallographic data for **1** and **2** in the LS and HS states.

	[Fe(*pp*)Pd(CN)$_4$]·G (1)		[Fe(*pp*)Pt(CN)$_4$]·G (2)	
Temperature (K)	293	125	293	123
Spin State	HS	LS	HS	LS
Empirical Formula *	$C_{10}H_4FeN_8Pd$	$C_{10}H_4FeN_8Pd$	$C_{10}H_4FeN_8Pt$	$C_{10}H_4FeN_8Pt$
M_r	398.46	398.46	487.15	487.15
Crystal System	monoclinic	monoclinic	monoclinic	monoclinic
Space Group	$P2/m$	$P2/m$	$P2/m$	$P2/m$
a (Å)	7.1903(3)	7.0619(6)	7.1806(5)	7.0971(6)
b (Å)	7.4599(2)	7.1811(5)	7.4575(5)	7.2163(4)
c (Å)	8.4271(4)	8.6859(7)	8.4389(8)	8.7642(8)
β (°)	107.071(5)	112.392(10)	107.185(9)	112.610(10)
V (Å^3)	432.11(3)	407.27(6)	431.72(6)	414.36(6)
Z	1	1	1	1
ρ_{calc} (g cm^{-3})	1.531	1.625	1.874	1.952
μ (mm^{-1})	1.880	1.995	8.933	9.307
Total Solvent Accessible Volume/Cell (Å^3)	159.1	146.5	160.0	149.3
Solvent Electrons/Cell	35.2	33.6	35.2	13.4
Goodness-of-Fit on F^2	1.065	1.059	0.891	1.019
Final R Indexes [$I >= 2\sigma(I)$]	$R_1 = 0.0251$, $wR_2 = 0.0588$	$R_1 = 0.0425$, $wR_2 = 0.0886$	$R_1 = 0.0373$, $wR_2 = 0.0585$	$R_1 = 0.0359$, $wR_2 = 0.0737$
Final R Indexes ** [All Data]	$R_1 = 0.0309$, $wR_2 = 0.0606$	$R_1 = 0.0469$, $wR_2 = 0.0905$	$R_1 = 0.0383$, $wR_2 = 0.0593$	$R_1 = 0.0367$, $wR_2 = 0.0744$
CCDC Number	2212767	2212768	2212765	2212766

* *Disordered water and methanol guest molecules (G) were masked upon the refinement.* ** $R_1 = \Sigma||F_o| - |F_c||/\Sigma|F_o|$ and $wR_2 = \{\Sigma[w(F_o^2 - F_c^2)^2]/\Sigma[w(F_o^2)^2]\}^{1/2}$ for $F_o^2 > 2\sigma(F_o^2)$.

Table 2. Selected structural parameters of **1** and **2**.

	[Fe(*pp*)Pd(CN)$_4$]·G (1)		[Fe(*pp*)Pt(CN)$_4$]·G (2)	
Temperature (K)	293	125	293	123
Spin State	HS	LS	HS	LS
<Fe−N>$_{average}$ (Å)	2.168(2)	1.953(3)	2.163(5)	1.961(5)
<Fe−N>$_{pp}$ (Å)	2.204(2)	1.976(3)	2.199(5)	1.980(5)
<Fe−N>$_{CN}$ (Å)	2.150(2)	1.942(3)	2.145(4)	1.951(4)
Fe···Fe between Adjacent Layers (Å)	9.335(1)	8.865(1)	9.326(1)	8.908(1)
$V_{oct}(FeN_6)$ (Å^3)	13.536	9.916	13.454	10.028
Σ (°)	32.0	21.2	27.3	24.0
$\angle$ M−C≡N (°)	4.1	6.5	2.1	5.4
$\angle$ Fe−N≡C (°)	20.7	12.7	22.9	13.0

It was found that both complexes crystallize in the monoclinic $P2/m$ space group, which is maintained after the spin transition. There is only one crystallographically independent iron(II) site in both HS and LS structures. It should be noted that analogous SCO compounds belonging to the same space group have also already been reported. For example, Hofmann-type clathrates with the composition [Fe(*bpb*)M(CN)$_4$]·xGuest (where M = Ni, Pt; Guest = (trifluoromethyl)benzene) display complete one-step SCO [33]. Another exam-

ple is the HS form of [Fe(*pz*)Pt(CN)$_4$]·*pz* stabilized by the inclusion of a pyrazine molecule in the framework as a guest molecule [24,29]. However, most similar frameworks with pillar ligands such as *pz*, *bpeben*, *dpe*, *azpy*, and *bpac* crystallize in the tetragonal *P*4/*mmm* space group [23,24,26–28,36–38,40,41].

In the title complexes, iron(II) has a coordination environment of an elongated FeN$_6$ pseudo-octahedron (Figure 1a). The equatorial positions of the octahedron are occupied by four N atoms of four crystallographically equivalent square-planar [M(CN)$_4$]$^{2-}$ (M = Pt, Pd) linkers generating corrugated 2D {FeM(CN)$_4$}$_\infty$ layers with (4,4)-net topology which lay in the *ab* plane. Cyanometallic layers lay one on top of each other and are supported by bridging *pp* ligands, which occupy the axial positions of iron(II). Thus, a porous 3D Hofmann-type framework (Figure 1b–d) is formed by analogy with complexes based on pyrazine [21].
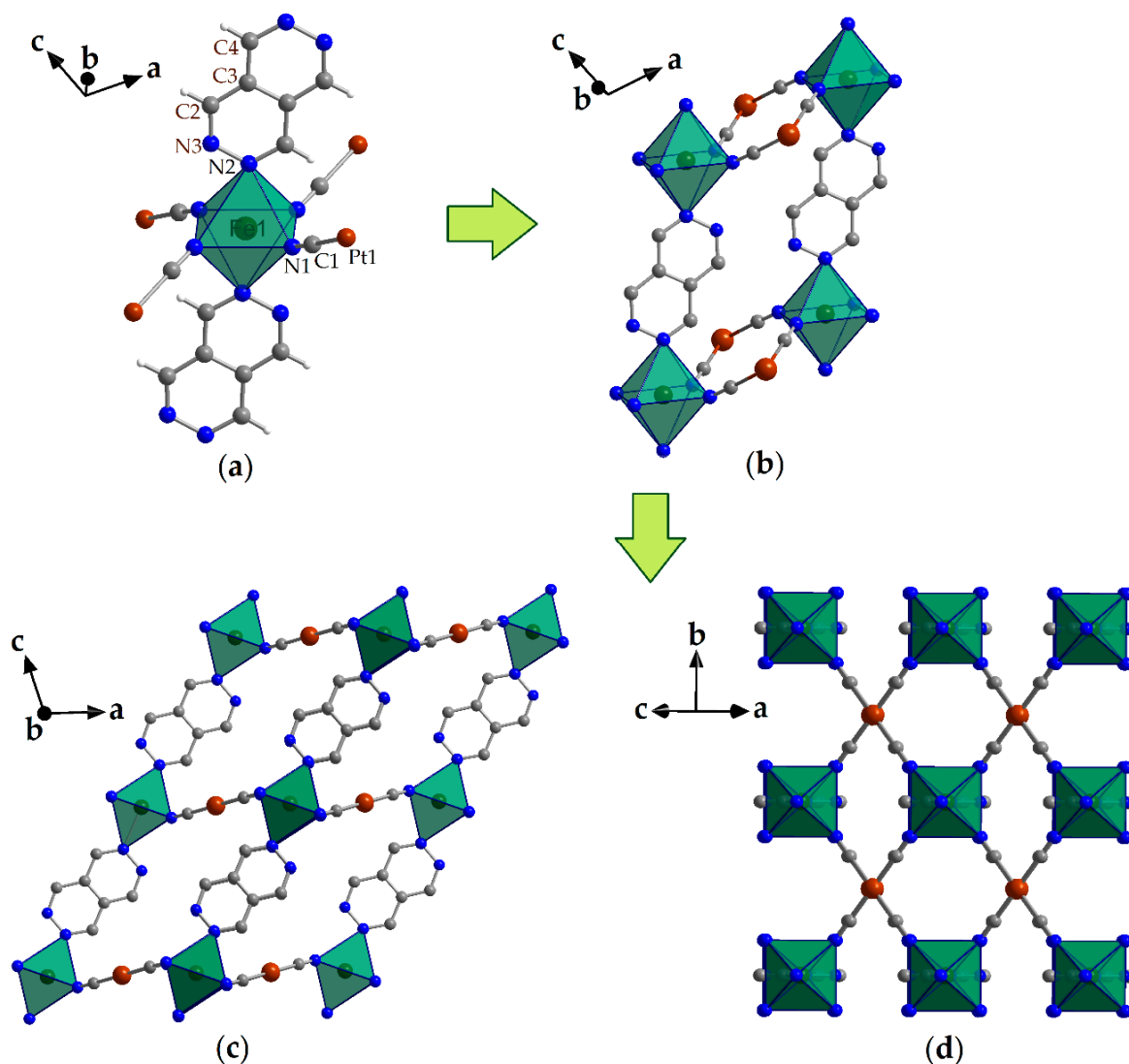

Figure 1. Crystal structure of [Fe(*pp*)Pt(CN)$_4$] (**2**) in the HS state: (**a**) Representation of a key fragment showing the coordination environment of iron(II); (**b**) The basic cavity of the structure; (**c**) View along *b* direction showing the corrugated cyanometallic layers and pillar coordination of these layers by *pp* ligands; (**d**) View in *ab* plane showing the 2D {FePt(CN)$_4$}$_\infty$ layer with (4,4)-net topology. Colour code: Fe (olive green), Pt (brown), N (blue), C (gray). Hydrogen atoms in (**b**–**d**) are omitted for clarity. Guest solvent molecules were removed.

Structural changes in the coordination environment of the metal are observed during a thermally induced spin transition. Changes in the unit cell parameters for both complexes

upon LS to HS transition are Δa = +1.8%, Δb = +3.9%, Δc = −3.0% for **1** and Δa = +1.2%, Δb = +3.3%, Δc = −3.7% for **2**. As a result, expansion along the *a* and *b* axes and contraction along the *c* axis are observed. The Fe−N≡C angles deviate from 180° by 20.7° (293 K) and 12.7° (125 K) for **1** and 22.9° (293 K) and 13.0° (123 K) for **2**. Such large values of Fe−N≡C angles clearly confirm the significant corrugation of the cyanometallic layers for both complexes. The M−C≡N angles deviate from linearity by 4.1° (293 K) and 6.5° (125 K) for $[Pd(CN)_4]^{2-}$ and 2.1° (293 K) and 5.4° (123 K) for $[Pt(CN)_4]^{2-}$. The C−M−C angles of both complexes do not change with temperature and are equal to 180°.

At 293 K, the average <Fe−N> bond lengths are 2.168(2) Å for **1** and 2.163(5) Å for **2**, which correspond to the HS state of iron(II) ions. A decrease in temperature to 123 K leads to the shortening of the average <Fe−N> bond lengths by about 0.2 Å to 1.953(3) Å for **1** and 1.961(5) Å for **2**, which is consistent with complete HS to LS transitions. Comparing the equatorial and axial Fe−N bond lengths, we notice that the former is always slightly shorter than the latter in both HS and LS states. The total change of the volume of the unit cell is 6.1% and 4.2% for **1** and **2**, respectively. As expected, the volume of the FeN_6 octahedron drops from 13.536 to 9.916 Å^3 for **1** and from 13.454 to 10.028 Å^3 for **2** upon HS to LS transitions.

The geometry around the iron(II) centres is sensitive to temperature change, and more precisely to the spin state of the iron(II) ions. At 293 K, the iron(II) octahedral distortion parameters (the sum of deviations from 90° for 12 "*cis*" N−Fe−N angles of FeN_6 octahedron) are Σ_{HS} = 32.0° for **1** and Σ_{HS} = 27.3° for **2**. At 123 K, the Σ_{LS} is reduced to 21.2° and 24.0° for **1** and **2**, respectively. Thus, LS iron(II) is characterized by a more regular FeN_6 octahedron with more linear coordination of cyanide ligands due to stronger Fe–N bonds.

The gate size of the pores in these SCO-PCPs is defined by the Fe···Fe distances through the pillar *pp* ligand and the $[M(CN)_4]^{2-}$ linkers (Figure S1). For **1** it is 9.34 × 7.19−7.46 Å in the HS state and 8.87 × 7.06–7.18 Å in the LS state. For **2** it is 9.33 × 7.18–7.46 Å in the HS state and 8.91 × 7.10–7.22 Å in the LS state. As expected, guest solvent molecules used for crystallization (H_2O and CH_3OH) are located inside the available pores of both complexes. However, we are unable to propose any reasonable structural model for them in the pores since they are highly disordered, even at 124 K. Therefore, electron density of guest solvent molecules was removed by the solvent mask routine. Although the removal of guest solvents with this procedure excludes the visualization of possible host-guest interactions and reduces some quality of the structural model, we note that this did not affect the general conclusions made regarding the topology of the frameworks, as well as the correct interpretation of the SCO behaviour of these PCPs.

The total number of electrons corresponding to solvent molecules per unit cell is 35.2 at 293 K and 33.6 at 125 K for **1** and 35.2 at 293 K and 13.4 at 123 K for **2**. The total solvent accessible volume per unit cell without considering the disordered solvent molecules for **1** was calculated as 159.1 Å^3 at 293 K and 146.5 Å^3 at 125 K, which corresponds to 36.8% and 36.0% of the unit-cell volume, respectively. For **2**, it was calculated as 160.0 Å^3 (37.1%) at 293 K and 149.3 Å^3 (36.0%) at 123 K (Table 2). As a result, an almost twofold increase in porosity is observed compared to the [Fe(*pz*)Pt(CN)$_4$] framework, for which the solvent-accessible voids in the HS and LS states are 90.4 Å^3 (22.4%) and 63.4 Å^3 (18.1%), respectively [24]. However, it should be noted that to date, Hofmann-type SCO-PCPs of the general formula [Fe(*L*)Pt(CN)$_4$] have already been obtained based on ligands of various sizes and chemical nature with larger values of the solvent-accessible voids: 849.6 Å^3 (53.8%) for *bpb* [31,33], 707.1 Å^3 (47.1%) for *dpsme* [35], 511 Å^3 (48.9%) for *bpeben* [36], 293.6 Å^3 (41.7%) for *bpac* [37,38], 286 Å^3 (43%) *azpy* [40], 272.7 Å^3 (39.8%) for *dpe* [41] (all these values are given for the LS state of the complexes since, unlike *pp* derivatives, most crystals of these compounds deteriorate rapidly during X-ray diffraction experiments at RT).

The preparation of bulk samples with described phases appeared to be a problematic task, which is why the SCO behaviour of both complexes was confirmed by variable-temperature single-crystal X-ray diffraction (SCXRD) experiments. This approach was used

due to the difficulty of collecting enough crystals for magnetic measurement, which is the most convenient method for monitoring SCO. The temperature dependences of the crystal lattice parameters of **1** and **2** are shown in Figures 2 and S2.
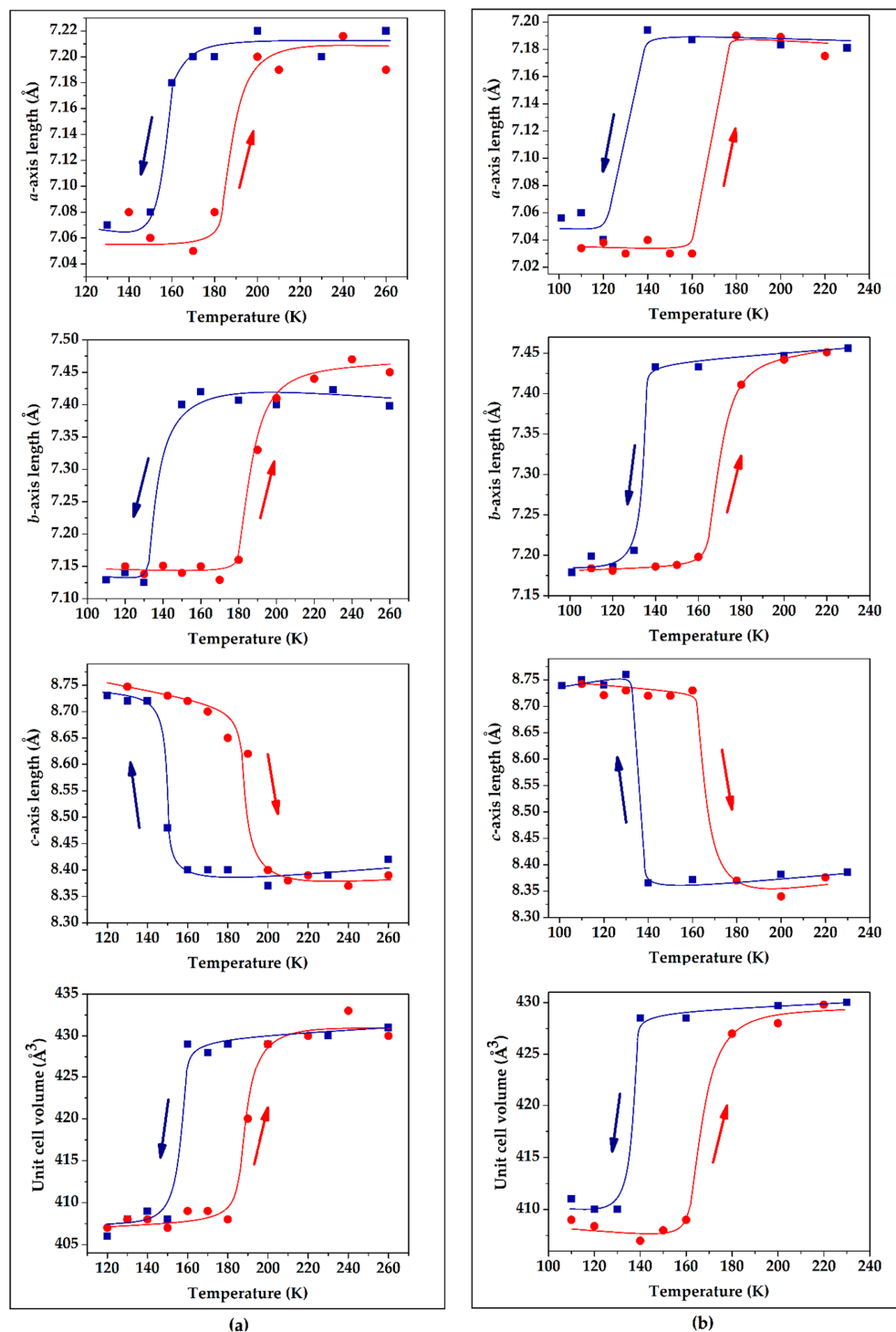

Figure 2. Temperature dependences of the crystal lattice parameters (*a* axis, *b* axis, *c* axis, and unit cell volume) of **1** (**a**) and **2** (**b**) upon heating (•) and cooling (■).

As expected, the crystallographic parameters change from LS to HS. There is a positive thermal expansion along *a* and *b* axes, while a negative thermal expansion takes place along *c* axis. From 120 to 200 K, the *a* and *b* parameters expand by ~2% and ~4%, respectively, while the *c* axis shrinks by ~4% for both complexes. This indicates the strong coupling

of the spin transition and lattice expansion/contraction. The total change of the volume of the unit cell is ∼5% for both complexes. Thus, the microscopic structural changes of the single crystal provoke its significant macroscopic changes, which is an important feature of the obtained compounds since it can be used for the development of molecular machines [61]. While most magnetic measurements are usually done in a sweep mode, the current diffraction measurements were performed in a settle regime. Thus, one should consider the small fluctuation upon thermalization at each temperature that can cause the width of obtained hysteresis loops to be slightly underestimated.

We attempted to explain the possible reason of these lattice deformations for both complexes by overlaying their crystal structures in the LS and HS states (Figure 3). If the expansion along the *a* and *b* axes can be explained by the increases in the molecular volume and Fe−N bond lengths upon LS to HS transitions (Figure 3a,b), then the contraction of the lattice along the *c* axis has some specific reason. There is a slightly different crystal packing of *pp* ligands along the *c* axis. Consequently, this SCO-driven packing of *pp* ligands leads to anisotropic expansion along the *b* axis and contraction along the *c* axis, as shown in Figure 3c,d.
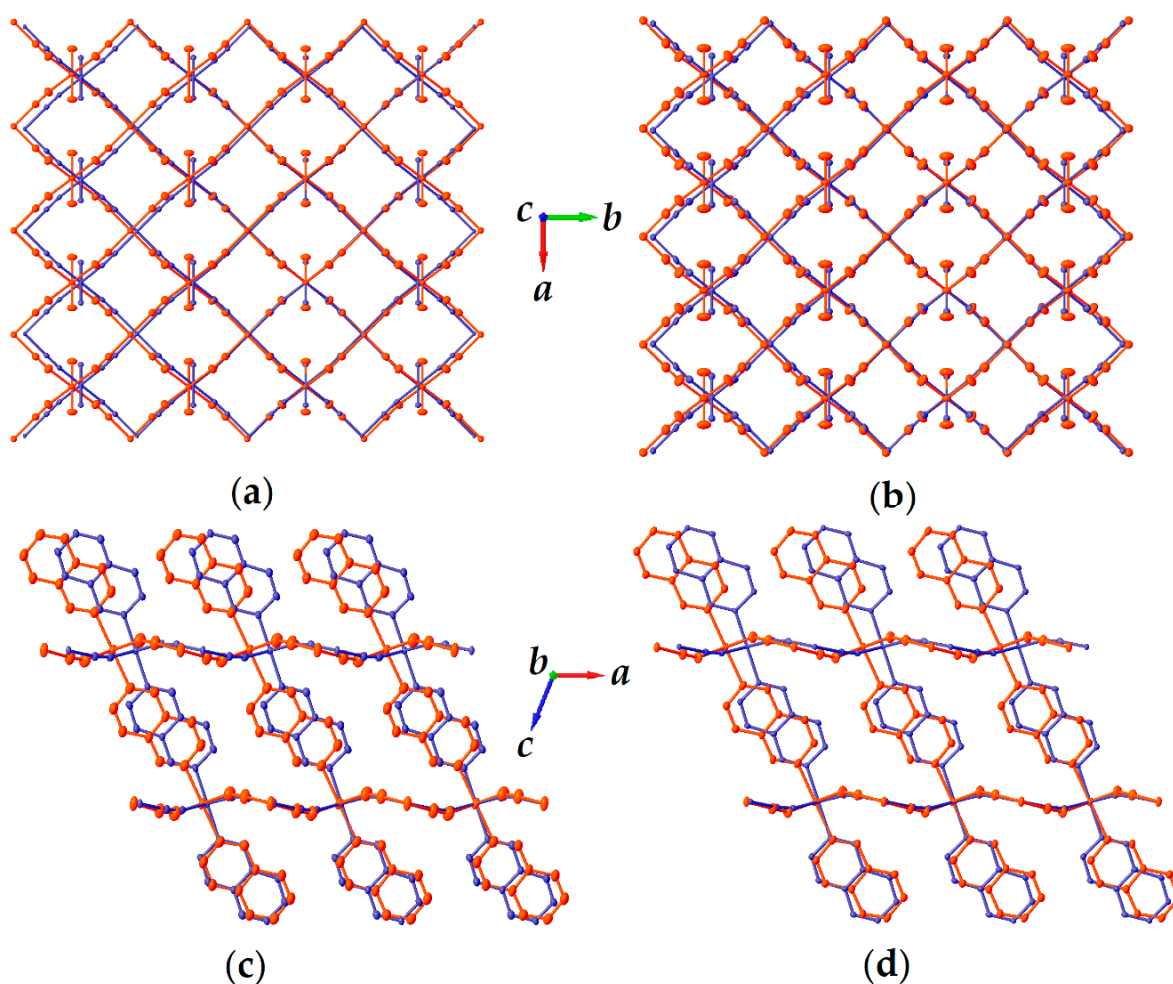

Figure 3. Superimposition of the LS (blue) and HS (red) sub-lattices of **1** (**a**,**c**) and **2** (**b**,**d**) along the *c*-axis and *b*-axis directions. Hydrogen atoms and disordered solvent are omitted for clarity.

The average value of transition temperatures for all crystal lattice parameters in the cooling/heating regimes are ca. 150/190 K and 135/170 K for **1** and **2**, respectively. The width of the thermal hysteresis loop is ca. 40 K for **1** and 35 K for **2**. The observed hysteresis loop is almost twice as wide as the desolvated [Fe(pz)Pt(CN)$_4$] framework, which is characterized by a 24 K hysteresis centred at 295 K (T$_{1/2}$↓ = 285 K and T$_{1/2}$↑ = 309 K) [24].

The presence of a wide thermal hysteresis loop clearly demonstrates the existence of a significant level of cooperativity for the single crystals of both *pp* complexes.

3. Materials and Methods

Single crystals of **1** and **2** were formed by a slow diffusion method within three layers in a 5 mL tube. $K_2[M(CN)_4]$ (where M = Pd, Pt) (0.010 mmol) and *pp* (0.025 mmol) in water (1 mL) from one side and $Fe(OTs)_2 \cdot 6H_2O$ (0.010 mmol) in methanol (1 mL) from another side were left to diffuse through a layer of water–methanol (1:1, 2 mL) for 3 weeks.

The crystal structures of **1** and **2** were determined by single-crystal X-ray diffraction using an Oxford-Diffraction XCALIBUR E CCD diffractometer (Oxford Diffraction Ltd., Abingdon, Oxfordshire, UK) with graphite-monochromated Mo-Kα radiation at 293/125 K for **1** and 293/123 K for **2**. SCXRD experiments in the form of pre-experiments were carried out in cooling and heating regimes on a selected single crystal at various temperatures (Tables S1 and S2). Data collection at low temperatures was performed using an Oxford Instruments open-flow N_2 Cryostream (Oxford Cryosystems Ltd., Long Hanborough, Oxford, UK) for cooling. The unit cell determination and data integration were carried out using the CrysAlisPro package from Oxford Diffraction (Yarnton, Oxfordshire, UK). Absorption correction using spherical harmonics was applied. The structures were solved by intrinsic phasing methods with SHELXT and refined by full-matrix least-squares on F^2 with SHELXL using the graphical interface of Olex2 (SHELX program from Institute of Inorganic Chemistry, Göttingen, Germany and Olex2 software from Durham University/EPSRC, Durham, UK) [62–64]. A solvent mask procedure integrated in Olex2 was used to remove the electron density from MeOH and H_2O guest molecules. All non-hydrogen atoms were refined anisotropically. Aromatic hydrogen atoms were geometrically fixed and refined using a riding model. Crystallographic data for **1** and **2** are listed in Tables S3–S32. Specific details of each refinement are given in the crystallographic information files (CIF-files). Crystallographic data for the structures have been deposited with the Cambridge Crystallographic Data Centre, CCDC: 2212767 (**1**—293 K), 2212768 (**1**—125 K), 2212765 (**2**—293 K), and 2212766 (**2**—123 K). Graphical representations of the structures were produced using Diamond 3.1 software (Crystal Impact GbR, Bonn, Germany). The distortion parameters (Σ) were calculated using the OctaDist tool (OctaDist development team: the Computational Chemistry Research Unit at Thammasat University (Pathum Thani, Thailand), the Functional Materials and Nanotechnology Center of Excellence at Walailak University (Thasala, Nakhon Si Thammarat, Thailand) and the Switchable Molecules and Materials group at University of Bordeaux (Nouvelle-Aquitaine, Bordeaux, France)) [65].

4. Conclusions

In this work, we have reported the synthesis and structural studies of two SCO-PCPs based on the *pp* ligand. Complexes **1** and **2** are isostructural to each other and display strong cooperative SCO behaviour with a wide thermal hysteresis loop at low temperatures. Due to the use of a more extended ligand (*pp*), obtained complexes show a twofold increase in porosity compared to the well-studied PCP [Fe(*pz*)Pt(CN)$_4$]. The total solvent accessible volume of **1** and **2** are about 160 Å^3 per iron(II) ion, which corresponds to 37% of the unit cell volume.

This research shows how the combination of SCO properties and high porosity makes *pp* complexes attractive multifunctional elements for various applications and implies their use as objects of further study on the influence of the guest effect on SCO behaviour including guest detection and separation studies.

Supplementary Materials: The following supporting information can be downloaded at: https://www.mdpi.com/article/10.3390/inorganics10110195/s1, Figure S1: View of the 1D channel of **1** (**a**) and **2** (**b**) along the *a*-axis direction. The gate sizes of the pores of **1** and **2** in the LS (blue) and HS (red) states; Figure S2: Temperature dependences of β angles of **1** (**a**) and **2** (**b**); Table S1: Selected crystallographic data for **1** extracted from SCXRD pre-experiments at various temperatures; Table S2:

Selected crystallographic data for **2** extracted from SCXRD pre-experiments at various temperatures.; Crystallographic data for **1** and **2** are listed in Tables S3–S32.

Author Contributions: V.M.H.: Conceptualization, Methodology, Formal analysis, Investigation, Visualization. S.S.: Methodology, Formal analysis, Investigation. K.V.D.: Formal analysis, Investigation. I.A.G.: Conceptualization, Methodology, Formal analysis, Investigation, Supervision. All authors have read and agreed to the published version of the manuscript.

Data Availability Statement: Crystallographic data are freely available at the Cambridge Crystallographic Data Centre under 2212765-2212768.

Conflicts of Interest: The authors declare no conflict of interest.

References

1. Gütlich, P.; Goodwin, H.A. (Eds.) *Spin Crossover in Transition Metal Compounds I–III*; Topics in Current Chemistry; Springer: Berlin, Germany, 2004.
2. Muñoz, M.C.; Real, J.A. Thermo-, piezo-, photo- and chemo-switchable spin crossover iron(II)-metallocyanate based coordination polymers. *Coord. Chem. Rev.* **2011**, *255*, 2068–2093. [CrossRef]
3. Gütlich, P.; Gaspar, A.B.; Garcia, Y. Spin state switching in iron coordination compounds. *Beilstein J. Org. Chem.* **2013**, *9*, 342–391. [CrossRef] [PubMed]
4. Kucheriv, O.I.; Fritsky, I.O.; Gural'skiy, I.A. Spin crossover in Fe^{II} cyanometallic frameworks. *Inorg. Chim. Acta* **2021**, *521*, 120303. [CrossRef]
5. Cirera, J. Guest effect on spin-crossover frameworks. *Rev. Inorg. Chem.* **2014**, *34*, 199–216. [CrossRef]
6. Ni, Z.-P.; Liu, J.-L.; Hoque, M.N.; Liu, W.; Li, J.-Y.; Chen, Y.-C.; Tong, M.-L. Recent advances in guest effects on spin-crossover behavior in Hofmann-type metal-organic frameworks. *Coord. Chem. Rev.* **2017**, *335*, 28–43. [CrossRef]
7. Murphy, M.J.; Zenere, K.A.; Ragon, F.; Southon, P.D.; Kepert, C.J.; Neville, S.M. Guest Programmable Multlstep Spin Crossover in a Porous 2-D Hofmann-Type Material. *J. Am. Chem. Soc.* **2017**, *139*, 1330–1335. [CrossRef] [PubMed]
8. Liu, W.; Peng, Y.; Wu, S.; Chen, Y.-C.; Hoque, M.N.; Ni, Z.; Chen, X.; Tong, M.-L. Guest-Switchable Multi-Step Spin Transitions in an Amine-Functionalized Metal-Organic Framework. *Angew. Chem. Int. Ed.* **2017**, *129*, 15178–15182. [CrossRef]
9. Piñeiro-López, L.; Valverde-Muñoz, F.-J.; Trzop, E.; Muñoz, M.C.; Seredyuk, M.; Castells-Gil, J.; da Silva, I.; Martí-Gastaldo, C.; Collet, E.; Real, J.A. Guest induced reversible on–off switching of elastic frustration in a 3D spin crossover coordination polymer with room temperature hysteretic behaviour. *Chem. Sci.* **2021**, *12*, 1317–1326. [CrossRef]
10. Létard, J.-F.; Guionneau, P.; Goux-Capes, L. Towards Spin Crossover Applications. In *Spin Crossover in Transition Metal Compounds III*; Topics in Current Chemistry; Gütlich, P., Goodwin, H.A., Eds.; Springer: Berlin, Germany, 2004; pp. 221–249.
11. Bousseksou, A.; Molnár, G.; Salmon, L.; Nicolazzi, W. Molecular spin crossover phenomenon: Recent achievements and prospects. *Chem. Soc. Rev.* **2011**, *40*, 3313. [CrossRef]
12. Real, J.A.; Andres, E.; Munoz, M.C.; Julve, M.; Granier, T.; Bousseksou, A.; Varret, F. Spin Crossover in a Catenane Supramolecular System. *Science* **1995**, *268*, 265–267. [CrossRef]
13. Romero-Morcillo, T.; De la Pinta, N.; Callejo, L.M.; Piñeiro-López, L.; Muñoz, M.C.; Madariaga, G.; Ferrer, S.; Breczewski, T.; Cortés, R.; Real, J.A. Nanoporosity, Inclusion Chemistry, and Spin Crossover in Orthogonally Interlocked Two-Dimensional Metal-Organic Frameworks. *Chem. Eur. J.* **2015**, *21*, 12112–12120. [CrossRef] [PubMed]
14. De La Pinta, N.; Klar, P.B.; Breczewski, T.; Madariaga, G. Host Polytypism and Structural Modulation in Two-Dimensional Fe(NCS)$_2$-Based Metal–Organic Frameworks: Can Spin-Crossover Transitions Be Predicted? *Cryst. Growth Des.* **2020**, *20*, 422–433. [CrossRef]
15. Orellana-Silla, A.; Valverde-Muñoz, F.J.; Muñoz, M.C.; Bartual-Murgui, C.; Ferrer, S.; Real, J.A. Halobenzene Clathrates of the Porous Metal–Organic Spin-Crossover Framework [Fe(tvp)$_2$(NCS)$_2$]$_n$. Stabilization of a Four-Step Transition. *Inorg. Chem.* **2022**, *61*, 4484–4493. [CrossRef]
16. Noro, S.; Kondo, M.; Ishii, T.; Kitagawa, S.; Matsuzaka, H. Syntheses and crystal structures of iron co-ordination polymers with 4,4′-bipyridine (4,4′-bpy) and 4,4′-azopyridine (azpy). Two-dimensional networks supported by hydrogen bonding, {[Fe(azpy)(NCS)$_2$(MeOH)$_2$]·azpy}$_n$ and {[Fe(4,4′-bpy)(NCS)$_2$(H2O)$_2$]·4,4′-bpy}$_n$. *J. Chem. Soc. Dalton Trans.* **1999**, *10*, 1569–1574. [CrossRef]
17. Halder, G.J. Guest-Dependent Spin Crossover in a Nanoporous Molecular Framework Material. *Science* **2002**, *298*, 1762–1765. [CrossRef] [PubMed]

18. Neville, S.M.; Moubaraki, B.; Murray, K.S.; Kepert, C.J. A Thermal Spin Transition in a Nanoporous Iron(II) Coordination Framework Material. *Angew. Chem. Int. Ed.* **2007**, *46*, 2059–2062. [CrossRef] [PubMed]

19. Neville, S.M.; Halder, G.J.; Chapman, K.W.; Duriska, M.B.; Moubaraki, B.; Murray, K.S.; Kepert, C.J. Guest Tunable Structure and Spin Crossover Properties in a Nanoporous Coordination Framework Material. *J. Am. Chem. Soc.* **2009**, *131*, 12106–12108. [CrossRef]

20. Neville, S.M.; Halder, G.J.; Chapman, K.W.; Duriska, M.B.; Southon, P.D.; Cashion, J.D.; Létard, J.-F.; Moubaraki, B.; Murray, K.S.; Kepert, C.J. Single-Crystal to Single-Crystal Structural Transformation and Photomagnetic Properties of a Porous Iron(II) Spin-Crossover Framework. *J. Am. Chem. Soc.* **2008**, *130*, 2869–2876. [CrossRef]

21. Niel, V.; Martinez-Agudo, J.M.; Muñoz, M.C.; Gaspar, A.B.; Real, J.A. Cooperative Spin Crossover Behavior in Cyanide-Bridged Fe(II)−M(II) Bimetallic 3D Hofmann-like Networks (M = Ni, Pd, and Pt). *Inorg. Chem.* **2001**, *40*, 3838–3839. [CrossRef]

22. Southon, P.D.; Liu, L.; Fellows, E.A.; Price, D.J.; Halder, G.J.; Chapman, K.W.; Moubaraki, B.; Murray, K.S.; Létard, J.-F.; Kepert, C.J. Dynamic Interplay between Spin-Crossover and Host−Guest Function in a Nanoporous Metal−Organic Framework Material. *J. Am. Chem. Soc.* **2009**, *131*, 10998–11009. [CrossRef]

23. Agustí, G.; Ohtani, R.; Yoneda, K.; Gaspar, A.B.; Ohba, M.; Sánchez-Royo, J.F.; Muñoz, M.C.; Kitagawa, S.; Real, J.A. Oxidative Addition of Halogens on Open Metal Sites in a Microporous Spin-Crossover Coordination Polymer. *Angew. Chem. Int. Ed.* **2009**, *48*, 8944–8947. [CrossRef] [PubMed]

24. Ohba, M.; Yoneda, K.; Agustí, G.; Muñoz, M.C.; Gaspar, A.B.; Real, J.A.; Yamasaki, M.; Ando, H.; Nakao, Y.; Sakaki, S.; et al. Bidirectional Chemo-Switching of Spin State in a Microporous Framework. *Angew. Chem. Int. Ed.* **2009**, *48*, 4767–4771. [CrossRef] [PubMed]

25. Ohtani, R.; Yoneda, K.; Furukawa, S.; Horike, N.; Kitagawa, S.; Gaspar, A.B.; Muñoz, M.C.; Real, J.A.; Ohba, M. Precise Control and Consecutive Modulation of Spin Transition Temperature Using Chemical Migration in Porous Coordination Polymers. *J. Am. Chem. Soc.* **2011**, *133*, 8600–8605. [CrossRef] [PubMed]

26. Muñoz Lara, F.J.; Gaspar, A.B.; Aravena, D.; Ruiz, E.; Muñoz, M.C.; Ohba, M.; Ohtani, R.; Kitagawa, S.; Real, J.A. Enhanced bistability by guest inclusion in Fe(II) spin crossover porous coordination polymers. *Chem. Commun.* **2012**, *48*, 4686. [CrossRef]

27. Arcís-Castillo, Z.; Muñoz-Lara, F.J.; Muñoz, M.C.; Aravena, D.; Gaspar, A.B.; Sánchez-Royo, J.F.; Ruiz, E.; Ohba, M.; Matsuda, R.; Kitagawa, S.; et al. Reversible Chemisorption of Sulfur Dioxide in a Spin Crossover Porous Coordination Polymer. *Inorg. Chem.* **2013**, *52*, 12777–12783. [CrossRef]

28. Aravena, D.; Castillo, Z.A.; Muñoz, M.C.; Gaspar, A.B.; Yoneda, K.; Ohtani, R.; Mishima, A.; Kitagawa, S.; Ohba, M.; Real, J.A.; et al. Guest modulation of spin-crossover transition temperature in a porous Iron(II) metal-organic framework: Experimental and periodic DFT studies. *Chem. Eur. J.* **2014**, *20*, 12864–12873. [CrossRef]

29. Polyzou, C.D.; Lalioti, N.; Psycharis, V.; Tangoulis, V. Guest induced hysteretic tristability in 3D pillared Hofmann-type microporous metal–organic frameworks. *New J. Chem.* **2017**, *41*, 12384–12387. [CrossRef]

30. Alvarado-Alvarado, D.; González-Estefan, J.H.; Flores, J.G.; Álvarez, J.R.; Aguilar-Pliego, J.; Islas-Jácome, A.; Chastanet, G.; González-Zamora, E.; Lara-García, H.A.; Alcántar-Vázquez, B.; et al. Water Adsorption Properties of Fe(pz)[Pt(CN)$_4$] and the Capture of CO$_2$ and CO. *Organometallics* **2020**, *39*, 949–955. [CrossRef]

31. Piñeiro-López, L.; Seredyuk, M.; Muñoz, M.C.; Real, J.A. Two- and one-step cooperative spin transitions in Hofmann-like clathrates with enhanced loading capacity. *Chem. Commun.* **2014**, *50*, 1833–1835. [CrossRef]

32. Piñeiro-López, L.; Valverde-Muñoz, F.J.; Seredyuk, M.; Muñoz, M.C.; Haukka, M.; Real, J.A. Guest Induced Strong Cooperative One- and Two-Step Spin Transitions in Highly Porous Iron(II) Hofmann-Type Metal–Organic Frameworks. *Inorg. Chem.* **2017**, *56*, 7038–7047. [CrossRef]

33. Piñeiro-López, L.; Seredyuk, M.; Muñoz, M.C.; Real, J.A. Effect of Guest Molecules on Spin Transition Temperature in Loaded Hofmann-Like Clathrates with Improved Porosity. *Eur. J. Inorg. Chem.* **2020**, *2020*, 764–769. [CrossRef]

34. Liu, F.-L.; Li, D.; Su, L.-J.; Tao, J. Reversible three equal-step spin crossover in an iron(II) Hofmann-type metal–organic framework. *Dalton Trans.* **2018**, *47*, 1407–1411. [CrossRef] [PubMed]

35. Sciortino, N.F.; Scherl-Gruenwald, K.R.; Chastanet, G.; Halder, G.J.; Chapman, K.W.; Létard, J.-F.; Kepert, C.J. Hysteretic Three-Step Spin Crossover in a Thermo- and Photochromic 3D Pillared Hofmann-type Metal–Organic Framework. *Angew. Chem. Int. Ed.* **2012**, *51*, 10154–10158. [CrossRef] [PubMed]

36. Muñoz-Lara, F.J.; Gaspar, A.B.; Muñoz, M.C.; Ksenofontov, V.; Real, J.A. Novel Iron(II) Microporous Spin-Crossover Coordination Polymers with Enhanced Pore Size. *Inorg. Chem.* **2013**, *52*, 3–5. [CrossRef]

37. Bartual-Murgui, C.; Ortega-Villar, N.A.; Shepherd, H.J.; Muñoz, M.C.; Salmon, L.; Molnár, G.; Bousseksou, A.; Real, J.A. Enhanced porosity in a new 3D Hofmann-like network exhibiting humidity sensitive cooperative spin transitions at room temperature. *J. Mater. Chem.* **2011**, *21*, 7217. [CrossRef]

38. Bartual-Murgui, C.; Salmon, L.; Akou, A.; Ortega-Villar, N.A.; Shepherd, H.J.; Muñoz, M.C.; Molnár, G.; Real, J.A.; Bousseksou, A. Synergetic Effect of Host–Guest Chemistry and Spin Crossover in 3D Hofmann-like Metal–Organic Frameworks [Fe(bpac)M(CN)$_4$] (M=Pt, Pd, Ni). *Chem. Eur. J.* **2012**, *18*, 507–516. [CrossRef]

39. Bartual-Murgui, C.; Akou, A.; Shepherd, H.J.; Molnár, G.; Real, J.A.; Salmon, L.; Bousseksou, A. Tunable Spin-Crossover Behavior of the Hofmann-like Network {Fe(bpac)[Pt(CN)$_4$]} through Host–Guest Chemistry. *Chem. Eur. J.* **2013**, *19*, 15036–15043. [CrossRef]

40. Agustí, G.; Cobo, S.; Gaspar, A.B.; Molnár, G.; Moussa, N.O.; Szilágyi, P.Á.; Pálfi, V.; Vieu, C.; Muñoz, M.C.; Real, J.A.; et al. Thermal and Light-Induced Spin Crossover Phenomena in New 3D Hofmann-Like Microporous Metalorganic Frameworks Produced As Bulk Materials and Nanopatterned Thin Films. *Chem. Mater.* **2008**, *20*, 6721–6732. [CrossRef]

41. Muñoz-Lara, F.J.; Gaspar, A.B.; Muñoz, M.C.; Arai, M.; Kitagawa, S.; Ohba, M.; Real, J.A. Sequestering Aromatic Molecules with a Spin-Crossover Fe^{II} Microporous Coordination Polymer. *Chem. Eur. J.* **2012**, *18*, 8013–8018. [CrossRef]

42. Shepherd, H.J.; Bartual-Murgui, C.; Molnár, G.; Real, J.A.; Muñoz, M.C.; Salmon, L.; Bousseksou, A. Thermal and pressure-induced spin crossover in a novel three-dimensional Hoffman-like clathrate complex. *New J. Chem.* **2011**, *35*, 1205. [CrossRef]

43. Arcís-Castillo, Z.; Muñoz, M.C.; Molnár, G.; Bousseksou, A.; Real, J.A. [Fe(TPT)$_{2/3}$\{M^I(CN)$_2$\}$_2$]·nSolv (M^I=Ag, Au): New Bimetallic Porous Coordination Polymers with Spin-Crossover Properties. *Chem. Eur. J.* **2013**, *19*, 6851–6861. [CrossRef] [PubMed]

44. Li, J.; Ni, Z.; Yan, Z.; Zhang, Z.; Chen, Y.; Liu, W.; Tong, M. Cyanide-bridged bimetallic 3D Hoffman-like coordination polymers with tunable magnetic behaviour. *Cryst. Eng. Comm.* **2014**, *16*, 6444–6449. [CrossRef]

45. Li, J.; Yan, Z.; Ni, Z.; Zhang, Z.; Chen, Y.; Liu, W.; Tong, M. Guest-Effected Spin-Crossover in a Novel Three-Dimensional Self-Penetrating Coordination Polymer with Permanent Porosity. *Inorg. Chem.* **2014**, *53*, 4039–4046. [CrossRef]

46. Clements, J.E.; Price, J.R.; Neville, S.M.; Kepert, C.J. Perturbation of Spin Crossover Behavior by Covalent Post-Synthetic Modification of a Porous Metal–Organic Framework. *Angew. Chem. Int. Ed.* **2014**, *53*, 10164–10168. [CrossRef] [PubMed]

47. Li, J.; Chen, Y.; Zhang, Z.; Liu, W.; Ni, Z.; Tong, M. Tuning the Spin-Crossover Behaviour of a Hydrogen-Accepting Porous Coordination Polymer by Hydrogen-Donating Guests. *Chem. Eur. J.* **2015**, *21*, 1645–1651. [CrossRef] [PubMed]

48. Li, J.-Y.; He, C.-T.; Chen, Y.-C.; Zhang, Z.-M.; Liu, W.; Ni, Z.-P.; Tong, M.-L. Tunable cooperativity in a spin-crossover Hoffman-like metal–organic framework material by aromatic guests. *J. Mater. Chem. C* **2015**, *3*, 7830–7835. [CrossRef]

49. Mullaney, B.R.; Goux-Capes, L.; Price, D.J.; Chastanet, G.; Létard, J.; Kepert, C.J. Spin crossover-induced colossal positive and negative thermal expansion in a nanoporous coordination framework material. *Nat. Commun.* **2017**, *8*, 1053. [CrossRef]

50. Meng, Y.; Dong, Y.; Yan, Z.; Chen, Y.; Song, X.; Li, Q.; Zhang, C.; Ni, Z.; Tong, M. A New Porous Three-Dimensional Iron(II) Coordination Polymer with Solvent-Induced Reversible Spin-Crossover Behavior. *Cryst. Growth Des.* **2018**, *18*, 5214–5219. [CrossRef]

51. Valverde-Muñoz, F.J.; Muñoz, M.C.; Ferrer, S.; Bartual-Murgui, C.; Real, J.A. Switchable Spin-Crossover Hofmann-Type 3D Coordination Polymers Based on Tri- and Tetratopic Ligands. *Inorg. Chem.* **2018**, *57*, 12195–12205. [CrossRef]

52. Li, Z.-Y.; Dai, J.-W.; Shiota, Y.; Yoshizawa, K.; Kanegawa, S.; Sato, O. Multi-Step Spin Crossover Accompanied by Symmetry Breaking in an Fe^{III} Complex: Crystallographic Evidence and DFT Studies. *Chem. Eur. J.* **2013**, *19*, 12948–12952. [CrossRef]

53. Ortega-Villar, N.; Muñoz, M.; Real, J. Symmetry Breaking in Iron(II) Spin-Crossover Molecular Crystals. *Magnetochemistry* **2016**, *2*, 16. [CrossRef]

54. Phonsri, W.; Davies, C.G.; Jameson, G.N.L.; Moubaraki, B.; Ward, J.S.; Kruger, P.E.; Chastanet, G.; Murray, K.S. Symmetry breaking above room temperature in an Fe(II) spin crossover complex with an N$_4$O$_2$ donor set. *Chem. Commun.* **2017**, *53*, 1374–1377. [CrossRef] [PubMed]

55. Zheng, C.; Jia, S.; Dong, Y.; Xu, J.; Sui, H.; Wang, F.; Li, D. Symmetry Breaking and Two-Step Spin-Crossover Behavior in Two Cyano-Bridged Mixed-Valence \{Fe$^{III}_2$(μ-CN)$_4$Fe$^{II}_2$\} Clusters. *Inorg. Chem.* **2019**, *58*, 14316–14324. [CrossRef] [PubMed]

56. Zhang, C.-J.; Lian, K.-T.; Huang, G.-Z.; Bala, S.; Ni, Z.-P.; Tong, M.-L. Hysteretic four-step spin-crossover in a 3D Hofmann-type metal–organic framework with aromatic guest. *Chem. Commun.* **2019**, *55*, 11033–11036. [CrossRef]

57. Zhang, C.-J.; Lian, K.-T.; Wu, S.-G.; Liu, Y.; Huang, G.-Z.; Ni, Z.-P.; Tong, M.-L. The substituent guest effect on four-step spin-crossover behavior. *Inorg. Chem. Front.* **2020**, *7*, 911–917. [CrossRef]

58. Kitase, K.; Kitazawa, T. A novel two-step Fe–Au type spin-crossover behavior in a Hofmann-type coordination complex \{Fe(4-methylpyrimidine)$_2$[Au(CN)$_2$]$_2$\}. *Dalton Trans.* **2020**, *49*, 12210–12214. [CrossRef]

59. Hiiuk, V.M.; Shylin, S.I.; Barakhtii, D.D.; Korytko, D.M.; Kotsyubynsky, V.O.; Rotaru, A.; Shova, S.; Gural'skiy, I.A. Two-Step Spin Crossover in Hofmann-Type Coordination Polymers [Fe(2-phenylpyrazine)$_2$\{M(CN)$_2$\}$_2$] (M = Ag, Au). *Inorg. Chem.* **2022**, *61*, 2093–2104. [CrossRef]

60. Domasevitch, K.V.; Solntsev, P.V.; Gural'skiy, I.A.; Krautscheid, H.; Rusanov, E.B.; Chernega, A.N.; Howard, J.A.K. Silver(I) ions bridged by pyridazine: Doubling the ligand functionality for the design of unusual 3D coordination frameworks. *Dalton Trans.* **2007**, *35*, 3893–3905. [CrossRef]

61. Shepherd, H.J.; Gural'skiy, I.A.; Quintero, C.M.; Tricard, S.; Salmon, L.; Molnár, G.; Bousseksou, A. Molecular actuators driven by cooperative spin-state switching. *Nat. Commun.* **2013**, *4*, 2607. [CrossRef] [PubMed]

62. Sheldrick, G.M. *SHELXT*—Integrated space-group and crystal-structure determination. *Acta Crystallogr. Sect. A Found. Adv.* **2015**, *71*, 3–8. [CrossRef]

63. Sheldrick, G.M. Crystal structure refinement with *SHELXL. Acta Crystallogr. Sect. C Struct. Chem.* **2015**, *71*, 3–8. [CrossRef]

64. Dolomanov, O.V.; Bourhis, L.J.; Gildea, R.J.; Howard, J.A.K.; Puschmann, H. *OLEX2*: A complete structure solution, refinement and analysis program. *J. Appl. Crystallogr.* **2009**, *42*, 339–341. [CrossRef]

65. Ketkaew, R.; Tantirungrotechai, Y.; Harding, P.; Chastanet, G.; Guionneau, P.; Marchivie, M.; Harding, D.J. OctaDist: A tool for calculating distortion parameters in spin crossover and coordination complexes. *Dalton Trans.* **2021**, *50*, 1086–1096. [CrossRef] [PubMed]